Holistic Comparison of Environmental Barrier Coating Material Candidates through Design of a Figure of Merit

Mackenzie J. Ridley* [1,2], Dominic J. Pinnisi[2], Elizabeth J. Opila[2]

[1]Oak Ridge National Laboratory, Corrosion Science and Technology, Oak Ridge, TN, USA

[2]University of Virginia, Materials Science and Engineering, Charlottesville, VA, USA

*Corresponding Author Contact: ridleymj@ornl.gov

Abstract: The first figure of merit for environmental barrier coating (EBC) materials was designed through a ranking system for material properties pertaining to established EBC failure modes in service. Seven past, present, and novel EBC candidate materials were used in the figure of merit design: SiO_2, $Ba_{0.75}Sr_{0.25}Al_2Si_2O_8$ (BSAS), $HfSiO_4$, $Yb_2Si_2O_7$, Yb_2SiO_5, Yb_2O_3, and $YbPO_4$. Utilizing compiled data from the literature, the presented figure of merit verified $Yb_2Si_2O_7$ as the state-of-the-art candidate with optimal EBC properties and infer that $YbPO_4$ should be considered as a potentially viable EBC material candidate. The figure of merit allows for holistic comparison of EBC candidates and informs experimental and computational search efforts for next generation complex EBCs. Clear knowledge gaps found through this work include CMAS-resistant coatings, EBC lifetimes before delamination, and oxidant diffusion rates in relevant EBC microstructures. It was shown that while some materials show promise for solving a single key failure mode for EBCs (i.e. CMAS reactivity), a community-wide goal should be placed on materials development to achieve acceptable resistance against all major failure modes, which are interconnected. Novel compositionally complex EBC materials, in addition to layered EBC architectures, show promise for optimization of material properties for long lifetime EBCs in combustion environments.

Keywords: Environmental barrier coatings, ceramic matrix composites, durability, figure of merit

Introduction

Silicon carbide ceramic matrix composites (SiC CMCs) are a novel technology for industrial gas turbine applications and have entered commercial aircraft use as of 2016 in the GE LEAP engine [1]. Environmental barrier coatings (EBCs) are required for application of CMCs at high temperatures to minimize SiC interaction with the combustion environment. EBC material design has focused on silicate materials to maintain chemical compatibility with both a

required silicon intermediate bond coat and the SiC. While EBCs are a supportive technology to enable CMC usage, an understanding of all EBC failure modes in service are critical for lifetime prediction of CMC components. The present review addresses the robust chemical, thermal, and mechanical stability requirements of EBCs and attempts to interconnect major failure modes through microstructural evolution from exposure to extreme turbine conditions.

The well-known failure modes for EBCs in service consist of the following: reactivity with steam, oxidation of the silicon bond coat, CaO-MgO-Al_2O_3-SiO_2 (CMAS) molten glass infiltration, thermal stresses, mechanical erosion, and foreign object damage [2]. Even though significant research is underway by many research teams on individual EBC failure modes, no holistic comparison or figure of merit (FoM) has been designed for EBC candidate materials. For example, the thermoelectric community utilizes a FoM for comparison of the Seebeck coefficient, electrical conductivity, and thermal conductivity with changes in temperature through a unified numerical value, ZT [3]. The complexity of EBCs limits the ability to produce a singular numerical model for comparison of EBC materials across all required intrinsic properties. However, a numerical ranking system and graphical FoM have been developed here for seven past, present, and novel EBC candidates, where normalized material properties were used to address the complex interconnectivity of material failure modes in combustion turbine environments.

1.0 Background

1.1 State-of-the-art

1.1.1 Gas Turbine Engine Conditions

The use of CMCs as hot section turbine components benefits fuel consumption through increased fuel burn temperatures above the melting temperatures of traditionally used Ni-base superalloy components with thermal barrier coatings (TBCs). For aerospace turbine applications, the lower material density of CMCs relative to superalloys leads to decreased component weight. CMC/EBC application are being pursued for static hot section components of gas turbines such as shrouds, combustor liners, and nozzles, as well as dynamic components such as turbine blades in the high-pressure regions of the engine [4], [5], [6]. Figure 1 displays the hot section of a Rolls-Royce turbofan, alongside expected environmental conditions in industrial gas turbines.

Operating conditions for the hot section of gas turbines can vary from 6 to 31 atm of pressure in high pressure turbine outlet and combustor outlet, respectively [7]. Typical gas temperatures after combustion can be 1100 °C - 1300 °C for commercial applications, depending on both position from the combustor outlet and stage of flight (take-off, cruise) [7], [8]. Turbine gas temperatures for Army applications routinely operate above 1400 °C with ongoing efforts to approach 1800 °C through additional support of component cooling channels and optimized CMC/EBC materials [6]. Fuel combustion results in approximately 10% partial pressure of H_2O (g) as a gaseous byproduct in the compressor region under high pressure, which translates to 0.6-3.1 atm of H_2O (g) [8], [9]. Gas velocities for a Model 501-K turbine (Rolls-Royce, Indianapolis, IN) have been measured to be 160 m/s-575 m/s from vane mid-span to the vane exit [8]. The gas velocity has also been calculated for a CFM56 turbine (CFM International, France) to range from 100-668 m/s, depending on distance from the combustor outlet [7]. Turbine conditions are further exacerbated during take-off and landing, where rapid temperature changes and pressures are placed on components. Land-based turbines for power generation may also require EBC/CMC systems in future designs due to an ongoing transition for replacement of natural gas fuels for low-carbon alternatives such as H_2 (g) of H_2 (g) blend fuels, where increased efficiencies (increased turbine inlet temperature and decreased reliance on cooling air) are likely needed to financially encourage the shift to cleaner energy sources. An expectation of increasing fuel burn temperatures for next generation gas turbines involves further adaptations in pressure and gas velocity values, yet component lifetimes greater than 25,000 hours have been proposed for both aero- and land-based turbine EBC/CMC systems for power generation [10], [11]. EBCs must therefore withstand extreme temperatures, pressures, gas chemistries, and gas velocities through multiple thermal cycles to support CMC components.

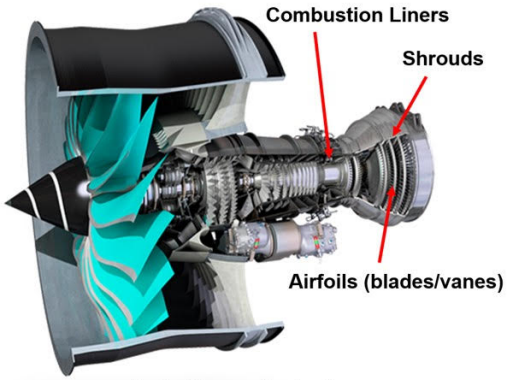

Temperature, °C	Pressure, atm	Gas velocity, m/s	$P(H_2O)$, atm
1100-1400 [6], [7], [8]	6-31 [7]	100-668 [7], [8]	0.1 [8]

Figure 1. Rolls-Royce Inc. Turbofan [12] and general industrial gas turbine environmental conditions.

1.1.2 EBC Processing

EBCs are typically applied to CMCs by atmospheric plasma spray (APS), where pre-reacted powder granule feedstock is ejected from a plasma onto the CMC/bond coat. EBC candidates are traditionally silicate ceramics to ensure chemical compatibility with SiC, Si, and SiO_2. The high velocities of the APS process induce a splat-like EBC microstructure along with cracks and porosity, where variations in phases and microstructure are possible primarily through controlling the plasma power via H_2 (g) flow [13]. While crystalline dense EBCs can be applied by APS with a heated substrate [14], commercial limitations of spraying into a furnace limit typical APS depositions to be performed on a cold substrate, resulting in an amorphous EBC with sometime non-equilibrium phases. For example, Garcia et al. have found presence of α-$Yb_2Si_2O_7$ and X1-phase Yb_2SiO_5 after APS deposition [15]. Equilibrium phases are established upon further heat treatment. Loss of SiO_2 from the powder interaction with the plasma results in silica deficient phases present, such as non-stoichiometric Yb_2SiO_5 and Yb_2O_3 [16]. An example of the sprayed EBC microstructure is shown for $Yb_2Si_2O_7$ in Figure 2 after annealing at 1200 °C for 2 hours in air [17]. Typical EBC thicknesses are around 100-300 µm thick, with the silicon bond coat being 25-75 µm. Upon heating, the EBC is crystallized and approaches equilibrium phase composition. Some degree of compressive stresses in the EBC are desired for adhesion and durability, which can be initially tailored through post-processing heat treatments. EBC candidate materials must be able to withstand the APS process without extensive decomposition and volatilization of components from interaction with the high temperature plasma.

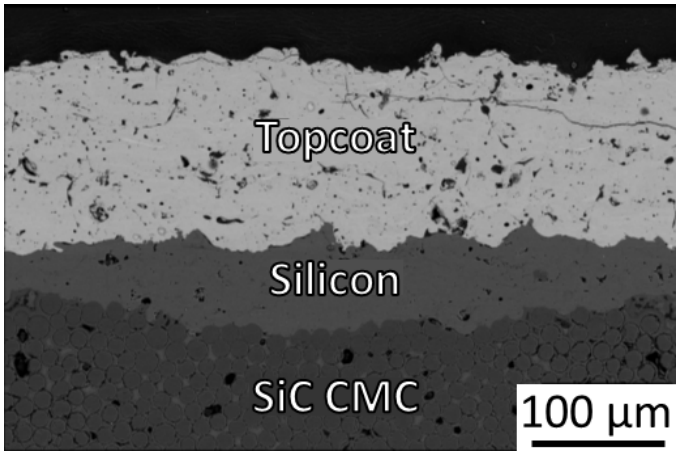

Figure 2. APS $Yb_2Si_2O_7$ topcoat with silicon bond coat on a SiC CMC substrate after annealing for 2h at 1200 °C in air [17].

1.2 EBC Failure Modes

Figure 3 relates EBC failure modes in service to the resultant phase distribution and microstructure from APS processing. Thermochemical (steam reaction, CMAS infiltration, and bond coat oxidation) and thermomechanical (thermal stresses, mechanical erosion, and foreign object damage) failure modes are all interconnected with each other as discussed below.

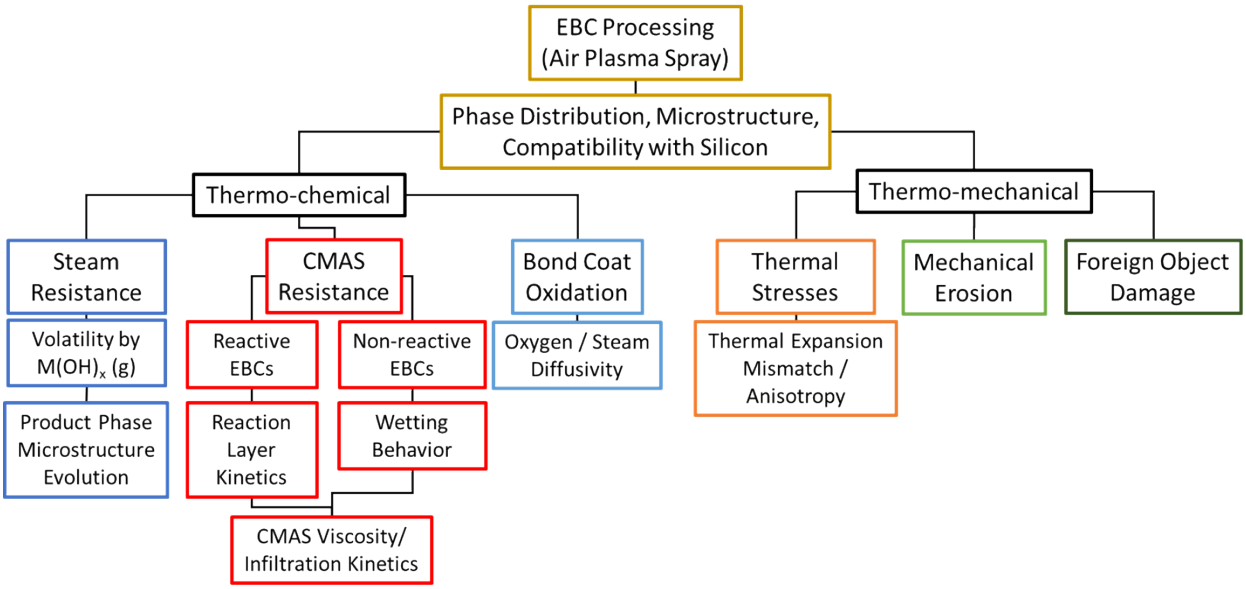

Figure 3. EBC failure modes and their respective causations.

1.2.1 Steam Resistance

Steam resistance is a vital characteristic of EBCs due to the known volatility of SiO_2, a thermally grown oxide (TGO) on SiC in a turbine environment. SiC is known to react with steam and produce a volatile silicon hydroxide gas species [9]. The volatilization of SiO_2 in steam leads to unacceptable recession rates of the SiC. EBCs must therefore provide additional steam resistance to support CMC technology, although the reaction kinetics and microstructural evolution of EBCs exposed to high-velocity water vapor are not yet fully understood. EBC candidates are often complex rare earth (RE) silicate compounds such as $RE_2O_3 \cdot 2SiO_2$ ($RE_2Si_2O_7$) where reactions with steam are expected to result in formation of $M_xO_yH_z$ metal hydroxide gas species. For example, the calculated partial pressures of primary hydroxide species for oxide constituents of $Y_2Si_2O_7$ (1200 °C: $Si(OH)_4$ (g) = $4x10^{-6}$ atm [18] and $Y(OH)_3$ (g) = $1x10^{-9}$ atm [19]) suggest that silica selectively volatilizes and leaves behind a silica-depleted and porous product phase. Such evidence has been found experimentally for many silicate EBC candidates [20], [21], [22], [23], [24], [25], [26]. EBC candidates thus should produce a reaction layer upon reaction with steam that is rich in an oxide that has very low volatility in a steam environment. State-of-the-art EBC $Yb_2Si_2O_7$ has been shown to undergo the following subsequent reactions in high-velocity steam:

$$Yb_2Si_2O_7 + 2H_2O\ (g) \rightarrow Yb_2SiO_5 + Si(OH)_4\ (g) + 24\%\ \text{porosity} \quad (1)$$

$$Yb_2SiO_5 + 2H_2O\ (g) \rightarrow Yb_2O_3 + Si(OH)_4\ (g) + 32\%\ \text{porosity} \quad (2)$$

where Yb_2O_3 does not display any measurable volatilization at 1400 °C [22]. Silicate EBC – steam reactions are controlled by a gas phase diffusion process, where a silicon hydroxide gas species diffusing out of the boundary layer represents the rate-limiting step in the reaction. Thus, production of a porous product layer inhibits further H_2O (g) transport to the EBC through an increase in the gas diffusion distance and leads to parabolic reaction kinetics, where the rate of volatilization decreases with increasing exposure time.

A cross-section scanning electron microscopy (SEM) image of $Yb_2Si_2O_7$ is shown in Figure 4 after exposure to 1 atm H_2O (g), 190-210 m/s steam for 250 hours at 1400 °C [22]. This image demonstrates the formation of reaction products Yb_2SiO_5 and Yb_2O_3 and associated porosity after exposure. Beneficial densification of the Yb_2SiO_5 microstructure further limited reactant transport to the $Yb_2Si_2O_7$ interface. Parabolic reaction kinetics were found for rare earth silicate reactions, where both time and velocity dependences suggest a diffusion-controlled

process through a gas boundary layer [22]. Through-cracking of the Yb_2SiO_5 reaction layer was indicative of the high thermal expansion anisotropy of Yb_2SiO_5, highlighting the interconnected relationship between thermochemical and thermochemical response.

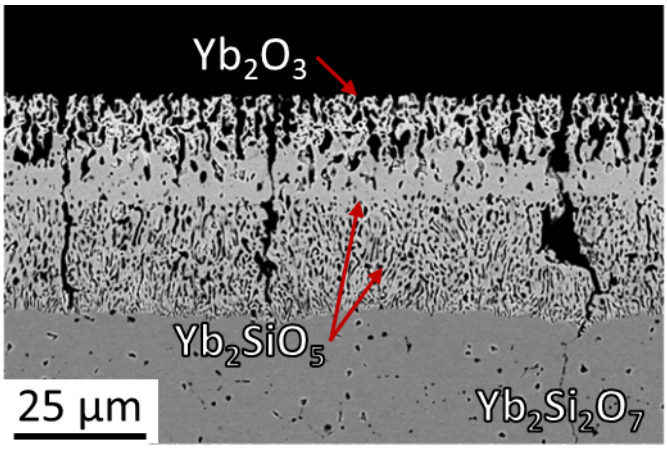

Figure 4. Backscattered electron SEM cross section of bulk $Yb_2Si_2O_7$ after a 1400 °C exposure to 1 atm $H_2O(g)$ at 190-210 m/s for 250 hours, adapted from [22].

Variability of high steam velocity and high steam partial pressure experimental setups results in significantly different product phase microstructures, kinetics, and impurity deposition from furnace ware [27], [28], [29], [30]. Thus, one approach to gauge steam reactivity is through measurement and comparison of a material's silica activity, $a(SiO_2)$. Table 1 presents the limited available silica activities for various EBC candidate materials, calculated from Thermo-Calc databases or measured by mass spectrometry. Both $RE_2Si_2O_7$ and RE_2SiO_5 phases display a clear decrease in $a(SiO_2)$, and thus steam reactivity, compared to uncoated SiC which has a silica activity of 1.

Table 1. Dual phase field silica activities for RE_2O_3-SiO_2 systems at 1673 K.

Rare Earth	$RE_2Si_2O_7$ - RE_2SiO_5	RE_2SiO_5 - RE_2O_3	Notes
Y	0.28	0.001	Mass spectrometry [31]
Y	0.085	0.00018	Thermo-Calc [32]
Yb	0.31	0.003	Mass spectrometry [33]
Lu	0.20	0.001	Mass spectrometry [34]
La	0.31	0.011	Thermo-Calc [32]

1.2.2 EBC Diffusivity/Silicon Bond Coat Oxidation Resistance

Oxidation of the silicon bond coat produces an amorphous SiO_2 film at the EBC/silicon interface. The formation of a thermally grown oxide (TGO) can cause new thermal stresses upon cycling. Thermal stresses can develop due to the very low thermal expansion coefficient of amorphous silica compared to the CMC, silicon bond coat, and EBC. Of utmost importance, amorphous silica can devitrify forming cristobalite during service, where a β- to α-phase transformation occurs around 270 °C with an associated 6% volume reduction, further damaging the EBC-bond coat interface [35]. EBC candidates should have low oxygen and water vapor diffusivity, where an industry limit has been placed at a maximum oxygen diffusion coefficient of $1x10^{-11}$ cm^2/s [36], assuming the oxidant can also quickly reach the bond coat through microstructural defects, such as porosity or cracks, resulting from either the APS process, the thermal stress release upon engine cycling, or from the porosity created with the EBC-steam reaction process.

Utilization of $^{18}O_2$ (g) for oxygen exchange studies is commonly used for determination of diffusion coefficients of high temperature materials [37], [38], [39]. Oxygen self-diffusion in bulk materials is lower than that of APS coatings and of materials in service, due to starting microstructural defects, induced thermal stress cracking, production of porosity upon EBC reaction with steam, and oxidant chemical potential gradients. No reliable published data are known for oxygen transport rates through APS deposited EBCs. Coated EBC-CMC systems are often compared against each other through cyclic furnace testing and direct measurement of thermally grown oxide formation at the EBC-Si or EBC-SiC interfaces [40], [41], [42]. In addition, high water vapor pressure in industrial gas turbines implies that oxidant transport to the interface may also be governed by water vapor. Wada et al. have shown that oxidant transport through phase pure $Yb_2Si_2O_7$ is increased in a water vapor environment compared to a dry oxygen environment [43]. Yet, oxidant transport rates and transport mechanisms through EBCs remain understudied (See panel 1) .

1.2.2 CMAS Resistance

Siliceous debris can be ingested to the engine during use as small particulate and are melted within the turbine. Due to the natural variability of ingested debris across the world, CaO-

MgO-Al_2O_3-SiO_2 (CMAS) molten glass can show a wide range of compositional variance in its primary components as well as in additional oxide constituents (Fe_2O_3, TiO_2, Na_2O, K_2O), leading to unique thermal properties of the glass [44], [45], [46]. Current safe gas turbine operating conditions are established at a concentration of ingested CMAS debris ≤0.002 g/m^3, which is considered below a visible concentration [47]. A CMAS loading estimation for coated hot section component determined from typical CMAS ingestion in the engine core in Dubai to be <1mg/cm^2 [48], [49], yet most commonly, experimental methods utilize an excessively high CMAS loading in the range of 10–40 mg/cm^2 to study the CMAS reaction process, crystallization behavior, and infiltration kinetics [50], [51], [52], [44], [53], [54]. With increasing engine operating temperatures, CMAS viscosity will decrease, such that CMAS reactivity could become more prevalent in the future as a primary EBC failure mode.

CMAS mitigation strategies are proposed in which EBCs are either reactive or unreactive with CMAS. The unreactive EBC approach relies on surface tension, similar to hydrophobicity, to limit CMAS reaction, repel molten CMAS from coating adherence, and keep the CMAS in the gas stream [55]. Reactive EBCs represent the more common mitigation approach. The EBC outer later becomes a sacrificial coating that promotes rapid formation of a CMAS reaction layer at the surface to produce a barrier for further CMAS ingress [53], [56], [57]. While CMAS – EBC reactions are complex, the primary reaction products are presented in Equation 3 and Equation 4 for Yb-silicate EBCs [53], [57], [58].

$$4Yb_2Si_2O_7 + 2CaO \rightarrow Ca_2Yb_8(SiO_4)_6O_2 + 2SiO_2 \quad (3)$$

$$4Yb_2SiO_5 + 2CaO + 2SiO_2 \rightarrow Ca_2Yb_8(SiO_4)_6O_2 \quad (4)$$

SEM cross-sections of state-of-the-art EBC $Yb_2Si_2O_7$ [59] and novel EBC candidate $YbPO_4$ [54] are presented on Figures 5 and 6, respectively, after exposure to ~40 mg/cm^2 of 33CaO-9MgO-13$AlO_{1.5}$-45SiO_2 (mol %) composition CMAS for 96 hours at 1300 °C. Both EBC materials react to form an apatite-type reaction product, although CMAS infiltration in the $Yb_2Si_2O_7$ tested by Webster and Opila rapidly occurred before a dense silicate apatite layer could form at the surface to prevent further CMAS ingress. Excessive infiltration of CMAS in $Yb_2Si_2O_7$ produces dilatation gradients, resulting in blister cracking and porosity production [57]. The $YbPO_4$ EBC candidate under the same conditions readily formed a dense $Ca_8MgYb(PO_4)_7$ apatite structure that effectively halted further CMAS infiltration, which can be seen by the large amount of residual glass left over on the $YbPO_4$ surface. The competing

kinetics of CMAS infiltration versus CMAS/EBC reaction rates has a clear connection to the ratio of CaO to SiO_2 in the CMAS melt, a common representative ratio for CMAS viscosity [59], [60], [61]. As stated earlier, the high CMAS loading used for both experiments are not expected to be seen for EBC components in service. The CMAS composition, loading rate, viscosity, and exposure temperature are thus vital parameters for determining stability of EBCs against molten CMAS attack.

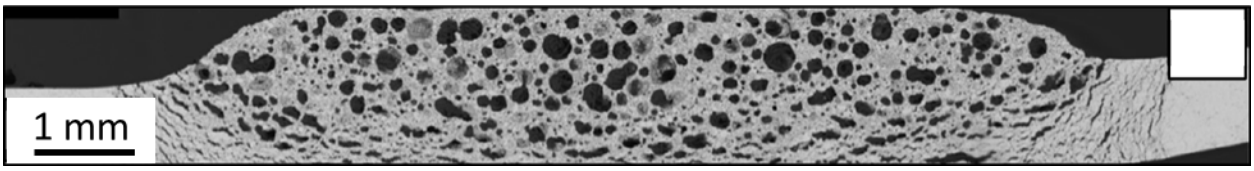

Figure 5. Phase-pure $Yb_2Si_2O_7$ after exposure to ~40 mg/cm² of $33CaO\text{-}9MgO\text{-}13AlO_{1.5}\text{-}45SiO_2$ composition CMAS for 96 hours at 1300 °C, adapted from [59].

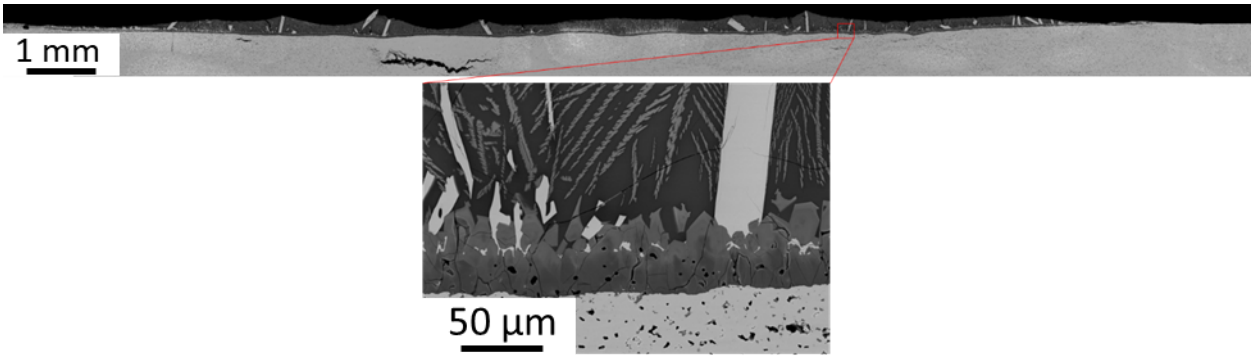

Figure 6. Phase-pure $YbPO_4$ after exposure to ~40 mg/cm² of $33CaO\text{-}9MgO\text{-}13AlO_{1.5}\text{-}45SiO_2$ (mol%) composition CMAS for 96 hours at 1300 °C, adapted from [54].

1.2.3 Thermal Stresses

Coefficient of thermal expansion (CTE) mismatch between the SiC CMC, silicon bond coat, thermally grown SiO_2, and the EBC can lead to stress buildup upon thermal cycling, inducing interfacial cracking and eventually material spallation. The CTEs of SiC, silicon, and thermally grown amorphous SiO_2 are 4.5-5.5x10^{-6} /°C [62], 3.5-4.5x10^{-6} /°C [63], and 0.5x10^{-6} /°C [64], respectively. Therefore, EBC candidates require a CTE in the general range of 3.5-6.5x10^{-6} /°C to minimize stress buildup at the EBC/silicon interface. EBC candidates typically have higher CTEs than SiC CMCs, resulting in tensile coating stresses upon cooling. While coating channel cracking from tensile stress may dominate as a thermal stress failure mode in pristine systems [65], the impact of the SiO_2 TGO on thermal stresses must also be considered.

As such, both EBC channel cracking from tensile stresses and EBC delamination from a growing TGO are primary concerns for EBC lifetimes which warrant further stress analyses.

The thermal expansion anisotropy of EBCs should be considered, as highly anisotropic EBCs will likely experience accelerated coating failure through microcracking. For example, the CTEs for monoclinic $Yb_2Si_2O_7$ are 5.6 x 10^{-6}/°C in the "a" direction and 2.8 x 10^{-6}/°C in the "c" direction (calculated from [66] based on XRD data up to 1600 °C) while CTEs for monoclinic Yb_2SiO_5 are 2.65 x 10^{-6}/°C in the "a" direction and 10.5 x 10^{-6}/°C in the "c" direction [67]. Yb_2SiO_5 and other RE_2SiO_5, displaying higher degrees of thermal expansion anisotropy [67], experience significant microcracking upon rapid changes in temperature [68], [69]. In Figure 4, Yb_2SiO_5 steam reaction product experienced stress cracking down to the $Yb_2Si_2O_7$ substrate even with the added compliance from surrounding porosity [22]. Microcracking upon thermal cycling represents yet another pathway for steam transport, oxidant transport, and CMAS infiltration towards the CMC.

1.2.4 Mechanical Erosion and Foreign Object Damage

Reaction products from both steam and CMAS interactions with EBCs can be present at the gas – EBC interface with increased porosity and cracking relative to the bulk EBC. Mechanical erosion of the EBC reaction layer(s) can result from a loss of structural integrity through introduction of excess porosity and cracking. Mechanical erosion was evident with the $HfSiO_4$ EBC candidate (Figure 7) during exposure to high velocity steam with residual liquid droplets for 250 hours at 1400 °C, where the erosion depth of the highly porous HfO_2 steam reaction product (~625 μm) exceeded that of typical EBC thicknesses in service (100-300 μm) at the 200-240 m/s velocity range [21]. In this process, the total thickness of the EBC is decreased over time, and unreacted EBC material is continually exposed to the turbine environment for further reaction or erosion. Solid particle erosion (SPE) studies have provided some clearer understanding of erosion rates for EBCs, although limited testing has been performed on EBC systems. Presby and Harder exposed $Yb_2Si_2O_7$ plasma sprayed EBCs to 100 – 150 m/s Al_2O_3 particulates in a burner rig at 1200°C [70]. It was found that the erosion rate was directly related to the particle kinetic energy (i.e. impact velocity and impact angle), and the trend also agreed with other literature sources for SPE testing on EBCs [71], [72].

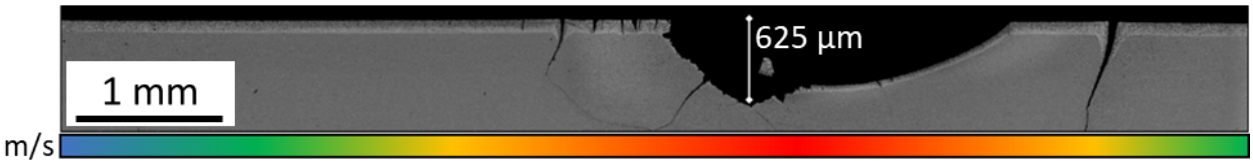

Figure 7. Backscattered electron SEM cross section of bulk $HfSiO_4$ after a 1400 °C exposure to 1atm $H_2O(g)$ for 250 hours. Excessive stress cracking and mechanical erosion of ~625 µm was measured at the impingement site (200-240 m/s water vapor velocity). Adapted from [21].

Foreign object damage (FOD) similarly results in EBC damage and erosion, although increased particulate sizes can introduce through-thickness cracking and localized spallation of material [73]. Choi analyzed FOD on uncoated SiC/SiC CMCs at both room temperature and 1316°C with steel ball projectiles impinging upon the specimens up to 440 m/s [74]. The CMCs showed greater resistance to FOD than monolithic ceramics due to the ability for the fibers to distribute kinetic energy through the system. Further, it has been shown that 3D fiber weaves can further dissipate impact energy and constrain damage better than 2D fiber weaves [75].

Upon particle impact with the application of an EBC, cone cracking and coating fragment ejection has been witnessed *in situ* by X-Ray radiography, where the EBC provides limited protection to the SiC substrate regarding crack propagation [76], [77]. Coating properties, such as density, hardness, and thickness, can be tailored to decrease total damage [78]. Hoffman et. al compared FOD to EBC coated hexaloy SiC with and without pre oxidation at 1316°C to grow a SiO_2 TGO [79]. Delamination occurred at the Si – SiC interface without introduction of a SiO_2 TGO and occurred through the TGO after oxidation exposure. While this effect may be due to changing EBC density and hardness after high-temperature exposures, the clear difference in failure mechanisms after oxidation testing exemplifies the importance of combined effects testing for multiple known EBC failure modes. Both erosion and FOD are dictated by the impact media (geometry, chemistry, hardness/density, size, impact angle, impact velocity) and the specimen properties (coating hardness/density, coating thickness, TGO thickness, interfacial roughness, monolithic vs. fiber composite substrates). The limited quantification on FOD and particulate erosion available in the literature, in addition to the complex nature of such studies, limits the ability to include mechanical erosion into the present Figure of Merit for EBC design.

2.0 EBC Figure of Merit

A FoM was developed utilizing the known failure modes of EBCs and the parameters in Table 2, gathered from the literature, which describe the phase stability, steam reactivity, CMAS reactivity, ability to act as an oxidant barrier, and thermal stresses induced for various past, present, and novel EBC material candidates. Here, SiO_2 is presented as the baseline material, as SiO_2 is the thermally grown oxide for both SiC and silicon without a protective EBC. Other materials for comparison include 2nd generation EBC $Ba_{0.75}Sr_{0.25}Al_2Si_2O_8$ (BSAS), $HfSiO_4$ (hafnon), Yb_2O_3, Yb_2SiO_5, state-of-the-art EBC $Yb_2Si_2O_7$, and novel EBC candidate $YbPO_4$.

Experimental and computational data were used to best fill in each material property in the table. Detailed explanation of provided data and data manipulation to develop the FoM can be found in supplementary materials. Due to the novelty of EBC materials research, many material properties listed are not yet available; approximations are noted below the table. For each failure mode category, a conditional value has been established as a method for appropriately differentiating between a successful (value = 0) and unsuccessful (value = 1) EBC candidate. For example, the presence of polymorphs is undesirable in the temperature range of interest to industrial gas turbines, as polymorph transitions include volume changes that induce material cracking. The conditional statement for *Phase Stability* assigns a value of 1 to crystalline SiO_2, which shows unfavorable polymorphs in the temperature range of interest. All other materials were assigned a value of 0, as they do not show unfavorable phase changes. In terms of *Thermal Stresses*, EBC CTEs with a value > 25% difference from the CTE of SiC ($5x10^{-6}$ /°C) are assigned a conditional binary value of 1 to demonstrate that the value of this property is unacceptable for a successful EBC.

Subcategories for *Phase Stability* are referenced from pseudo binary phase diagrams for each respective material. *Steam Reactivity* has been represented by three sub-categories. First, through the activity of the volatile component metal oxide species, such as the $a(SiO_2)$ for silicate EBC candidates or $a(P_2O_5)$ for the rare earth phosphates. Additionally, the amount of porosity produced upon steam reaction has been determined from known high-velocity (>50 m/s) water vapor chemical reactions. The steam reaction product melting temperature was also used to represent each steam product's phase stability.

CMAS Reactivity has been represented by the changes in CMAS viscosity upon reaction as a simple metric for both CMAS infiltration rates and EBC/CMAS reaction rates. A starting

SiO_2/CaO ratio of 45/33 was used, based on a common CMAS composition used in literature studies [50]. A conditional statement was used to favor EBCs that produce a protective reaction layer to prevent further CMAS ingress. *EBC Diffusivity and* resulting *Silicon Bond Coat Oxidation* was represented by the bulk EBC oxygen diffusion coefficients at 1400 °C in addition to a conditional statement based on the maximum diffusion coefficient standard already described [36]. Values of $-\log_{10}(D_{Bulk})$ were used as the input into the FoM so that all data can be compared without spanning multiple orders of magnitude. The *Thermal Stresses* represent thermo-mechanical behavior of EBCs and includes the CTE, CTE anisotropy of the EBC, and the CTE of the steam reaction product. A final conditional statement was used to ensure EBCs have minimal CTE mismatch with SiC.

*Table 2. Thermo-chemical and thermo-mechanical properties of selected high temperature coating materials. Conditional binary values are denoted with *.*

Thermo-chemical	**SiO_2**	**Yb_2O_3**	**Yb_2SiO_5**	**$Yb_2Si_2O_7$**	**BSAS**	**$HfSiO_4$**	**$YbPO_4$**
Phase Stability							
Melting point of EBC, °C	1723 [80]	2250 [81]	1950 [81]	1850 [81]	1680 [82]	1770 [83]	1896 [a] [84]
* More than one stable phase? Yes = 1, No = 0	1	0	0	0	0	0	0
Nearby eutectic temperature, °C	1723 [80]	1850 [81]	1850 [81]	1650 [81]	1300 [85]	1650 [83]	1450 [b] [86]
Steam Reactivity							
Oxide activity in H_2O (g), a(MO_x)	1 [9]	0 [c] [20]	0.003 [d] [33]	0.2 [e] [33]	1 [f] [87]	0.55 [88]	0.2 [g] [54]
Volume loss upon H_2O (g) reaction, %	100 [20]	0 [20]	32 [22]	24 [22]	100 [87]	45 [21]	44 [54]
Melting point of H_2O (g) reaction product	1723 [80]	2250 [81]	2250 [81]	1850 [81]	1680 [82]	2758 [83]	2250 [81]
* High-velocity H_2O (g) reaction kinetics, linear = 1, parabolic = 0	1 [20]	0 [c] [20]	0 [22]	0 [22]	1 [87]	0 [21]	0 [54]
CMAS Reactivity							
SiO_2/CaO ratio changes upon CMAS reaction	0.030 [h]	-0.106 [h]	0.023 [h]	0.152 [h]	0.061 [h]	0.030 [h]	0.436 [h]
* Formation of a protective reaction layer, Yes = 0, No = 1	1	0 [89], [90]	0 [53]	0 [53]	1 [91]	1 [92]	0 [54]

Bond Coat Oxidation							
O_2 (g) Self diffusion D_{Bulk} in EBC, 1400 °C, cm^2/s	$2.3x10^{-10}$ [93]	$8.0x10^{-12}$ **i** [94]	$8.3x10^{-14}$ [37]	$1.3x10^{-14}$ [38]	$4.7x10^{-15}$ **j** [36]	$1.3x10^{-14}$ **k** [95]	$1.3x10^{-14}$ **k** [95]
***** EBC requirement that $D_{Bulk}<1x10^{-11}$ cm^2/s, Yes = 0, No = 1	0	0	0	0	0	0	0
Thermo-mechanical	**SiO_2**	**Yb_2O_3**	**Yb_2SiO_5**	**$Yb_2Si_2O_7$**	**BSAS**	**$HfSiO_4$**	**$YbPO_4$**
Thermal stresses							
Linear CTE $x10^{-6}$ /°C	0.5 **l** [64]	8.4 [96]	7.25 [67]	4.5 [97]	5.3 [98]	4 [99]	6 [54]
CTE anisotropy, max-min CTE axes, $x10^{-6}$ /°C	0	0 [96]	8.1 [67]	2.5 [97]	2.6 **m** [100]	3 [99]	1.9 [54]
CTE of steam reaction product, $x10^{-6}$ /°C	0.5 **l** [64]	8.4 [96]	8.4 [96]	7.25 [67]	5.3 [98]	6.1 [101]	8.4 [96]
***** Is linear CTE of EBC within 25% of SiC (4.5-5.5 $x10^{-6}$ /°C), Yes = 0, No = 1	1	1	1	0	0	0	0

Table 3. Assumptions and clarifications to Table 2.

Assumptions and clarifications to Table 2 are as follows:

a: The $YbPO_4$ melting temperature is unknown. The $ErPO_4$ melt temperature [74] was used to estimate that of $YbPO_4$.

b: The Yb_2O_3-P_2O_5 phase diagram is unknown. The nearby eutectic temperature was estimated from the Y_2O_3-P_2O_5 phase diagram [76].

c: Volatility of Yb_2O_3 was estimated to be negligible based on high velocity steam testing of $Yb_2Si_2O_7$ [15] and high-velocity steam testing of Y_2O_3 [13].

d: The a(SiO_2) from the Yb_2O_3-Yb_2SiO_5 two-phase field was presented [33].

e: The a(SiO_2) from the Yb_2SiO_5-$Yb_2Si_2O_7$ two-phase field was presented [33].

f: The a(MOx) consists of all oxide constituents (BaO, SrO, Al_2O_3, SiO_2) since all components volatilize in high-velocity steam [78].

g: The a(P_2O_5) in rare earth orthophosphates is unknown. The a(P_2O_5) was assumed to be near 0.2 based on comparable reaction rates to $Yb_2Si_2O_7$ [54] in high-velocity steam testing at 1400 °C.

h: The SiO_2/CaO ratio changes were determined from consumption of a 45/33 ratio SiO_2/CaO CMAS upon EBC reaction and introduction of additional SiO_2 and/or CaO into the residual melt:

$$\frac{SiO_2}{CaO}\ Ratio\ Changes = \frac{(SiO_{2UCSB} - SiO_{2EBC\ Reaction})}{(CaO_{UCSB} - CaO_{EBC\ Reaction})}$$

The baseline CMAS composition used here was derived from commonly used synthetic CMAS [52] with a SiO_2/CaO ratio of 45/33. $HfSiO_4$ reaction with CMAS is unknown; $HfSiO_4$ was assumed to donate SiO_2 to the melt and not produce a reaction product, based on the reaction between CMAS and $ZrSiO_4$.

i: The bulk oxygen diffusion coefficient of Yb_2O_3 is unknown. The presented value was self-diffusion of single crystal Y_2O_3 at 1400 °C [84].

j: The oxygen diffusion coefficient of $Ba_{0.75}Sr_{0.25}Al_2Si_2O_8$ (BSAS) is unknown. The oxygen diffusion coefficient for $Al_6Si_2O_{13}$ (mullite) at 1400 °C was extrapolated from 1119 °C -1319 °C data [36] to be used as an estimate for BSAS.

k: The oxygen diffusion coefficient of $HfSiO_4$ and $YbPO_4$ are unknown. The oxygen diffusion coefficient for tetragonal $ZrSiO_4$ at 1400 °C [85] was used as an estimate for $HfSiO_4$ and $YbPO_4$ since all materials exhibit the same space group.

l: The CTE of amorphous SiO_2 at 1027 °C [64].

m: The BSAS CTE anisotropy is unknown. The CTE anisotropy for $BaAl_2Si_2O_8$ (BAS) [90] was used as an estimate for that of $Ba_{0.75}Sr_{0.25}Al_2Si_2O_8$ (BSAS).

Raw material property data from Table 2 were normalized between 0 and 1 for each subcategory. Each material property was scaled so that 0 and 1 represented the most desired and least desired material property value, respectively. These normalized values can be summed together for each material to receive a FoM score for each material, shown in Table 3, where a smaller score represents a better EBC material candidate. It was seen that $Yb_2Si_2O_7$ displayed the smallest FoM score, which implies that $Yb_2Si_2O_7$ is the optimum EBC candidate from the materials used in this study. Contrarily, SiO_2, which is representative of the SiC thermally grown oxide without an EBC, displayed the highest FoM score; the least desirable EBC material candidate. The novel non-silicate EBC candidate $YbPO_4$ displayed the same FoM score as state-of-the-art $Yb_2Si_2O_7$, although many assumptions were made for $YbPO_4$ due to the lack of material property data available in the literature.

Table 4. Figure of Merit score for each material, determined from summation of Table 2 after normalization of each subcategory with values from 0 to 1. Smaller FoM scores represent the most desirable EBC material candidate.

Figure of Merit Score						
SiO_2	Yb_2O_3	Yb_2SiO_5	$Yb_2Si_2O_7$	BSAS	$HfSiO_4$	$YbPO_4$
7.99	6.47	6.16	3.78	7.62	5.82	3.78

Each normalized subcategory can also be summed to produce numerical values for the categories of *Phase Stability*, *Steam Reactivity*, *CMAS Reactivity*, *Bond Coat Oxidation*, and *Thermal Stresses*. These groupings are plotted in Figure 3 as a radar plot. Smaller FoM scores for each leg of the plot represent a more desirable material property for EBC application. Thus, materials that encompass a smaller area of the plot are better EBC candidates. For example, Yb_2O_3 displays highly desired phase stability, steam resistance, and CMAS resistance, yet a standalone Yb_2O_3 EBC would be expected to quickly fail through its high thermal stresses and/or through gas transport to the EBC/Silicon bond coat interface for rapid SiO_2 TGO formation. Both $Yb_2Si_2O_7$ and $YbPO_4$ encompass the smallest areas on the plot, and thus represent the better EBC candidates of the materials presented here. The radar plot provides a visual representation for the FoM score results in Table 3, where EBC candidates can be holistically compared. It should be noted that the arrangement of properties around the circumference of the radar plot

affects the total encompassed area. Thus, the numerical FoM is more quantitative, whereas the plot provides easy visual comparison of EBC candidate material properties.

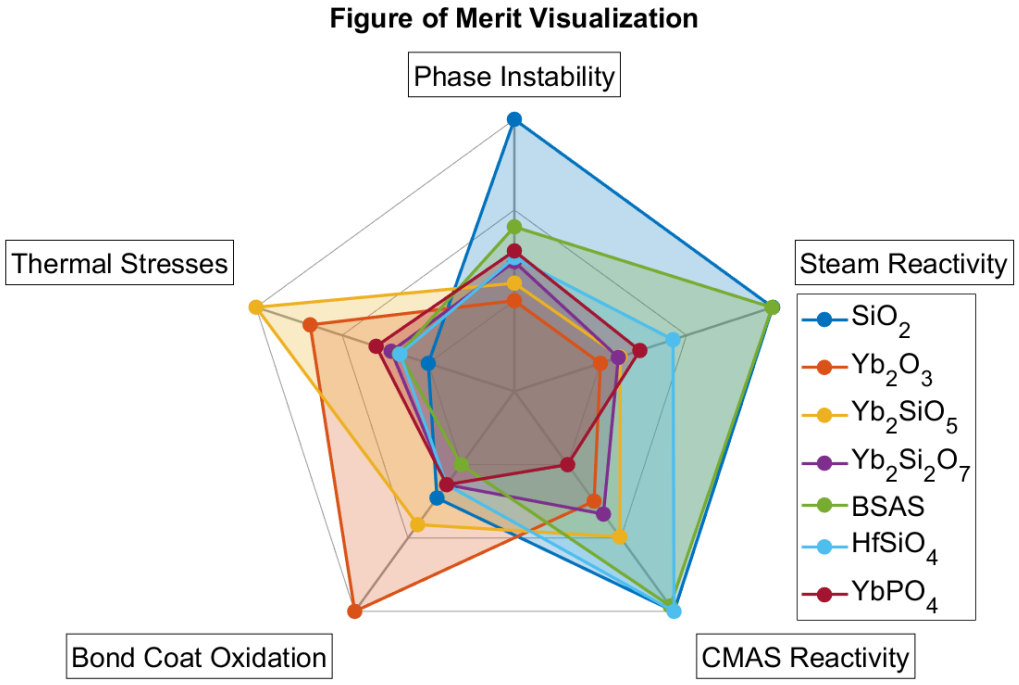

Figure 8. Figure of merit visualization for EBC material candidates. Smaller encompassed area on the figure indicates increased overall stability as an EBC material.

3.0 Discussion

Candidate materials in this study can be ranked from best to worst EBC candidates, based on Table 3 and Figure 8: $Yb_2Si_2O_7$, $YbPO_4$, Yb_2O_3, $HfSiO_4$, Yb_2SiO_5, BSAS, and SiO_2. The state-of-the-art EBC $Yb_2Si_2O_7$ is verified through Table 3 as the most desirable material candidate. $YbPO_4$, a novel EBC material, has the same FoM score as $Yb_2Si_2O_7$, which suggests $YbPO_4$ and other xenotime rare earth orthophosphates ($REPO_4$) should be further studied as EBC material candidates. Still, five of the 15 data inputs for $YbPO_4$ are unknown and were roughly estimated based on similar materials and experimental comparison. Further research is needed to accurately determine the data inputs for $YbPO_4$. Particularly, the Yb_2O_3-P_2O_5 phase diagram with material melting temperatures, the a(P_2O_5) value for $YbPO_4$, and the oxygen diffusion coefficient in $YbPO_4$ need to be determined for accurate ranking of $YbPO_4$ phase stability, steam reactivity, and oxidation resistance, respectively.

Of the materials used in this work, Yb_2O_3, $HfSiO_4$, Yb_2SiO_5, BSAS, and SiO_2 are known to be unacceptable single-layer EBC material candidates. The thermal expansion of Yb_2O_3 is far greater than that of SiC [96]. $HfSiO_4$ exposed to steam results in a highly porous and weakly connected HfO_2 reaction layer that undergoes mechanical erosion at gas velocities relevant to turbine conditions [21]. Yb_2SiO_5 has an unacceptably high CTE anisotropy that leads microcracking upon thermal cycling [67], [102]. BSAS reacts with SiO_2, the thermally grown oxide, to form a liquid eutectic at 1300 °C and therefore cannot be considered as an EBC due to this maximum use temperature [85]. Additionally, BSAS fully volatilizes in steam with linear reaction kinetics [85], [87], making BSAS coatings only suitable as an intermediate layer of protection between a lower EBC (stable with SiO_2) and an outer EBC (low volatility) multi-layer system. The use of legacy EBC material candidates in this study provides insight on acceptable material property values required for current generation EBCs and enables identification of missing EBC properties which should be studied.

Determination of a FoM for EBCs remains a challenge due to the complexity of the EBC failure modes and the lack of available data on high temperature ceramic materials for comparison. Incorporating high-temperature mechanical property data with thermal expansion mismatch between layers is required for an accurate depiction of thermal stress evolution with temperature cycling. Coating adhesion strengths and energy release rates are also considered important metrics for improving understanding of coating lifetimes in service. The steam reaction parameter should eventually incorporate kinetic data as well as information on microstructural evolution of the product phase, where various testing procedures can be compared through gas boundary layer theory. CMAS reaction thermodynamics, reaction kinetics, and infiltration kinetics are also needed information to further understand and compare EBC materials, although a defined CMAS loading and test methodology first should be established within the EBC community. In addition, reactions of EBCs with other molten deposits such as Na_2SO_4 also result in degradation and require additional study (Panel 2). EBC diffusivity data, and resulting silicon bond coat oxidation kinetics, are particularly lacking (Panel 1). Furthermore, H_2O (g) diffusion coefficients should be determined for all materials in phase-pure and APS condition, as water vapor partial pressures in turbine environments are 0.6-3.1 atm or greater. It is unknown if O_2 (g) or H_2O (g) represents the primary silicon oxidant in turbine environments, or how the complex microstructures produced from air plasma spray affect

oxidant transport. Finally, it must be stated that true EBC/CMC systems are expected to operate with a strong thermal gradient across the component, where most laboratory testing relies on isothermal exposures. Differences in performance are expected to occur with a temperature gradient, and likely could impact the resulting FoM correlations between material candidates.

Additional secondary properties of interest to EBC material performance should also be considered for the FoM, such as material thermal conductivity, modulus, and the processability by APS technique. The presented FoM shows promise for comparison of other high temperature materials such as thermal barrier coatings (TBCs) for use on superalloys and for EBCs on novel CMC designs, such as eutectic oxide-based CMCs.

The presented method for material comparison may prove useful for more similar materials, such as comparison of various rare earth disilicates ($RE_2Si_2O_7$) to the state-of-the-art $Yb_2Si_2O_7$ material. The oxide activities of all $RE_2Si_2O_7$ are not yet known, however it is known that variation of the rare earth cation results in a unique chemical resistance [103]. Future work certainly requires computational methods for both determination of material properties as well as prediction of materials that fit specified property requirements of EBCs. For instance, utilization of machine learning, deep learning, and artificial intelligence can allow for both improved understanding of leading failure mechanisms and guidance on material properties predictions for novel coating candidates, particularly when experimental and modeling efforts are combined into training sets for intelligence programs [104], [105], [106], [107]. The overall impact of tailoring EBC properties through cation substitutions in compositionally complex ceramics and high entropy ceramic materials, currently undergoing considerable research, should be quantified for inclusion in this FoM comparison [108], [109], [110], [111], [112], [42], [113], [114].

Novel materials should be compared against recognized EBCs first by the properties most easily measure in laboratories, such as CTE and phase stability, to encourage high-throughput materials development. Following a candidate's initial success, more involved properties can be analyzed, such as the effectiveness of a material to inhibit bond coat oxidation. Deposition of EBC candidates on SiC can be utilized for furnace cyclic testing to measure thermally grown oxide kinetics at the interface, although many factors can limit similitude between experimental setups. Thus, oxidant diffusivity data can be measured for EBC candidate materials as a simple metric for oxidation kinetics.

4.0 Conclusion

The first figure of merit for environmental barrier coating candidates was presented as a method for holistic comparison of materials against significant failure modes experienced by components in service. This simple model can be used alongside experimental, computational, and artificial intelligence methods to compare properties of known materials, determine avenues for future EBC research, and predict the reliability of complex materials in combustion environments. Of the seven materials utilized within the Figure of Merit, $Yb_2Si_2O_7$ was confirmed as the state-of-the-art EBC material of choice. $YbPO_4$, a novel EBC candidate, showed a high ranking within the Figure of Merit. As such, rare earth phosphates may be suitable as EBC materials and more investigation regarding material properties and performance are reasonable. This work clearly outlines known knowledge gaps in the field, such as oxidant diffusion rates, molten deposit reactivities, and coating adhesion strength as a function of high-temperature exposure. Compositionally complex EBCs represent a possible avenue for tailoring material properties to provide adequate resistance against all interconnected failure modes during service.

5.0 Acknowledgements

The authors would like to acknowledge the Office of Naval Research program manager Dr. David Shifler for funding this work under Award #N000141712280.

References

[1] J. Steibel, Z. Ren, G. Singh, A. Misra, K. N. Lee, and M. van Roode, "Ceramic matrix composites taking flight at GE aviation," *American Ceramic Society Bulletin*, no. 98, pp. 30–33, 2019.

[2] K. N. Lee, "$Yb_2Si_2O_7$ Environmental barrier coatings with reduced bond coat oxidation rates via chemical modifications for long life," *Journal of the American Ceramic Society*, vol. 102, no. 3, pp. 1507–1521, 2019, doi: https://doi.org/10.1111/jace.15978.

[3] G. D. Mahan, "Figure of merit for thermoelectrics," *Journal of Applied Physics*, vol. 65, no. 4, pp. 1578–1583, Feb. 1989, doi: 10.1063/1.342976.

[4] D. LaChapelle, M. Noe, W. Edmondson, H. Stegemiller, J. Steibel, and D. Chang, "CMC materials applications to gas turbine hot section components," in *34th AIAA/ASME/SAE/ASEE Joint Propulsion Conference and Exhibit*, American Institute of Aeronautics and Astronautics. doi: 10.2514/6.1998-3266.

[5] G. Gardiner, "Aeroengine Composites, Part 1: The CMC invasion," *Composites World*, 2015, [Online]. Available: compositesworld.com/articles/aeroengine-composites-part-1-the-cmc-invasion

[6] M. J. Walock, V. Heng, A. Nieto, A. Ghoshal, M. Murugan, and D. Driemeyer, "Ceramic Matrix Composite Materials for Engine Exhaust Systems on Next-Generation Vertical Lift Vehicles,"

Journal of Engineering for Gas Turbines and Power, vol. 140, no. 102101, Jun. 2018, doi: 10.1115/1.4040011.

[7] T. H. Nguyen, P. Tri Nguyen, and F. Garnier, "Evaluation of the relationship between the aerothermodynamic process and operational parameters in the high-pressure turbine of an aircraft engine," *Aerospace Science and Technology*, vol. 86, pp. 93–105, Mar. 2019, doi: 10.1016/j.ast.2019.01.011.

[8] M. K. Ferber and H. T. Lin, "Environmental Characterization of Monolithic Ceramics for Gas Turbine Applications," *Key Eng. Mat.*, vol. 287, pp. 367–380, Jun. 2005, doi: 10.4028/www.scientific.net/KEM.287.367.

[9] E. J. Opila and R. E. Hann, "Paralinear Oxidation of CVD SiC in Water Vapor," *Journal of the American Ceramic Society*, vol. 80, no. 1, pp. 197–205, 1997, doi: 10.1111/j.1151-2916.1997.tb02810.x.

[10] G. Lipiak and A. Schroeder, "Lifetime extension for Siemens gas turbines," *VGB PowerTech*, vol. 87, no. 10, Jul. 2007.

[11] K. L. More *et al.*, "Exposure of Ceramics and Ceramic Matrix Composites in Simulated and Actual Combustor Environments," presented at the ASME 1999 International Gas Turbine and Aeroengine Congress and Exhibition, American Society of Mechanical Engineers Digital Collection, Dec. 2014. doi: 10.1115/99-GT-292.

[12] "Rolls-Royce Inc." Accessed: Dec. 19, 2020. [Online]. Available: https://www.rolls-royce.com/

[13] E. Garcia, H. Lee, and S. Sampath, "Phase and microstructure evolution in plasma sprayed $Yb_2Si_2O_7$ coatings," *Journal of the European Ceramic Society*, vol. 39, no. 4, pp. 1477–1486, Apr. 2019, doi: 10.1016/j.jeurceramsoc.2018.11.018.

[14] B. T. Richards and H. N. G. Wadley, "Plasma spray deposition of tri-layer environmental barrier coatings," *Journal of the European Ceramic Society*, vol. 34, no. 12, pp. 3069–3083, Oct. 2014, doi: 10.1016/j.jeurceramsoc.2014.04.027.

[15] E. Garcia, O. Sotelo-Mazon, C. A. Poblano-Salas, G. Trapaga, and S. Sampath, "Characterization of Yb2Si2O7–Yb2SiO5 composite environmental barrier coatings resultant from in situ plasma spray processing," *Ceramics International*, vol. 46, no. 13, pp. 21328–21335, Sep. 2020, doi: 10.1016/j.ceramint.2020.05.228.

[16] J. Huang *et al.*, "Effect of deposition temperature on phase composition, morphology and mechanical properties of plasma-sprayed Yb2Si2O7 coating," *Journal of the European Ceramic Society*, p. S0955221921006130, Aug. 2021, doi: 10.1016/j.jeurceramsoc.2021.08.046.

[17] L. Herweyer, "The High Temperature Sodium Sulfate Interactions with Ytterbium Disilicate Environmental Barrier Coatings Systems and Silicon Carbide Ceramic Matrix Composite Materials," University of Virginia, 2020. doi: 10.18130/V3-XJEB-E003.

[18] P. J. Meschter, E. J. Opila, and N. S. Jacobson, "Water Vapor–Mediated Volatilization of High-Temperature Materials," *Annu. Rev. Mater. Res.*, vol. 43, no. 1, pp. 559–588, Jul. 2013, doi: 10.1146/annurev-matsci-071312-121636.

[19] C. W. Bauschlicher, C. J. Bodenschatz, D. L. Myers, and N. S. Jacobson, "Thermodynamics of high-temperature aluminum, zirconium, and yttrium hydroxide and oxyhydroxide vapor species," *Journal of the American Ceramic Society*, vol. 103, no. 10, pp. 5870–5880, 2020, doi: https://doi.org/10.1111/jace.17213.

[20] C. G. Parker and E. J. Opila, "Stability of the Y_2O_3-SiO_2 system in high-temperature, high-velocity water vapor," *J Am Ceram Soc*, p. jace.16915, Dec. 2019, doi: 10.1111/jace.16915.

[21] M. J. Ridley and E. J. Opila, "Thermomechanical and Thermochemical Stability of $HfSiO_4$ for Environmental Barrier Coating Applications," *J Am Ceram Soc*, 2020, doi: 10.1111/jace.17729.

[22] M. Ridley and E. Opila, “Thermochemical stability and microstructural evolution of $Yb_2Si_2O_7$ in high-velocity high-temperature water vapor,” *Journal of the European Ceramic Society*, vol. 41, no. 5, pp. 3141–3149, May 2020, doi: 10.1016/j.jeurceramsoc.2020.05.071.
[23] S. Ueno, T. Ohji, and H.-T. Lin, “Recession behavior of $Yb_2Si_2O_7$ phase under high speed steam jet at high temperatures,” *Corrosion Science*, vol. 50, no. 1, pp. 178–182, Jan. 2008, doi: 10.1016/j.corsci.2007.06.014.
[24] N. Al Nasiri, N. Patra, D. D. Jayaseelan, and W. E. Lee, “Water vapour corrosion of rare earth monosilicates for environmental barrier coating application,” *Ceramics International*, vol. 43, no. 10, pp. 7393–7400, Jul. 2017, doi: 10.1016/j.ceramint.2017.02.123.
[25] E. Bakan, M. Kindelmann, W. Kunz, H. Klemm, and R. Vaßen, “High-velocity water vapor corrosion of Yb-silicate: Sprayed vs. sintered body,” *Scripta Materialia*, vol. 178, pp. 468–471, 2020, doi: https://doi.org/10.1016/j.scriptamat.2019.12.019.
[26] M. J. Ridley and E. J. Opila, “Variable Thermochemical Stability of RE2Si2O7 (RE = Sc, Nd, Er, Yb, or Lu) in High-temperature High-velocity Steam,” *Journal of American Ceramic Society*, Aug. 2021, doi: 10.1111/jace.18120.
[27] K. N. Lee, D. S. Fox, and N. P. Bansal, “Rare earth silicate environmental barrier coatings for SiC/SiC composites and Si_3N_4 ceramics,” *Journal of the European Ceramic Society*, vol. 25, no. 10, pp. 1705–1715, Jan. 2005, doi: 10.1016/j.jeurceramsoc.2004.12.013.
[28] S. Ueno, D. D. Jayaseelan, H. Kita, T. Ohji, and H. T. Lin, “Comparison of Water Vapor Corrosion Behaviors of $Ln_2Si_2O_7$ (Ln=Yb and Lu) and $ASiO_4$ (A=Ti, Zr and Hf) EBC’s,” *Key Engineering Materials*, vol. 317–318, pp. 557–560, 2006, doi: 10.4028/www.scientific.net/KEM.317-318.557.
[29] H. Klemm, “Silicon Nitride for High-Temperature Applications,” *Journal of the American Ceramic Society*, vol. 93, no. 6, pp. 1501–1522, Jun. 2010, doi: 10.1111/j.1551-2916.2010.03839.x.
[30] N. Maier, K. G. Nickel, and G. Rixecker, “High temperature water vapour corrosion of rare earth disilicates $(Y,Yb,Lu)_2Si_2O_7$ in the presence of $Al(OH)_3$ impurities,” *Journal of the European Ceramic Society*, vol. 27, no. 7, pp. 2705–2713, Jan. 2007, doi: 10.1016/j.jeurceramsoc.2006.09.013.
[31] N. Jacobson, “Silica Activity Measurements in the Y_2O_3-SiO_2 System and Applications to Modeling of Coating Volatility,” *Journal of American Ceramic Society*, vol. 97, no. 6, pp. 1959–1965, 2014.
[32] *Thermo-calc Software TCOX Database Version 8*. Thermo-calc.
[33] C. Gustavo and N. S. Jacobson, “Mass spectrometric measurements of the silica activity in the Yb_2O_3–SiO_2 system and implications to assess the degradation of silicate-based coatings in combustion environments,” *Journal of the European Ceramic Society*, vol. 35, pp. 4259–4267, 2015.
[34] B. A. Kowalski, N. S. Jacobson, C. Bodenschatz, and G. Costa, “Thermodynamics of the Lu2O3 – SiO2 system and comparison to other rare earth silicates,” *The Journal of Chemical Thermodynamics*, vol. 161, p. 106483, Oct. 2021, doi: 10.1016/j.jct.2021.106483.
[35] M. J. Lance, M. J. Ridley, K. A. Kane, and B. A. Pint, “Raman spectroscopic characterization of SiO2 phase transformation and Si substrate stress relevant to EBC performance,” *Journal of the American Ceramic Society*, vol. 106, no. 10, pp. 6205–6210, 2023, doi: 10.1111/jace.19190.
[36] R. A. Golden, “Matric Development for Water Vapor Resistant SiC-Based Ceramic Matric Composites,” Dissertation, University of Virginia, Charlottesville, Virginia, 2017.
[37] T. Matsudaira *et al.*, “Mass transfer in polycrystalline ytterbium monosilicate under oxygen potential gradients at high temperatures,” *Journal of the European Ceramic Society*, Jul. 2020, doi: 10.1016/j.jeurceramsoc.2020.07.045.
[38] S. Kitaoka *et al.*, “Mass Transfer Mechanism in $Yb_2Si_2O_7$ Under Oxygen Potential Gradients at High Temperatures,” in *Advances in High Temperature Ceramic Matrix Compo sites and Materials for Sustainable Development; Ceramic Transactions, Volume CCLXIII*, John Wiley & Sons, Ltd, 2017, pp. 187–195. doi: 10.1002/9781119407270.ch19.

[39] F. Nozahic, C. Estournès, A. L. Carabat, W. G. Sloof, S. van der Zwaag, and D. Monceau, "Self-healing thermal barrier coating systems fabricated by spark plasma sintering," *Materials & Design*, vol. 143, pp. 204–213, Apr. 2018, doi: 10.1016/j.matdes.2018.02.001.
[40] K. Kane, E. Garcia, M. Lance, C. Parker, S. Sampath, and B. Pint, "Accelerated oxidation during 1350°C cycling of ytterbium silicate environmental barrier coatings," *J Am Ceram Soc.*, vol. 105, no. 4, pp. 2754–2763, Dec. 2021, doi: 10.1111/jace.18231.
[41] K. A. Kane *et al.*, "Evaluating steam oxidation kinetics of environmental barrier coatings," *J Am Ceram Soc*, vol. 105, no. 1, pp. 590–605, Jan. 2022, doi: 10.1111/jace.18093.
[42] M. Ridley *et al.*, "Steam oxidation and microstructural evolution of rare earth silicate environmental barrier coatings," *Journal of the American Ceramic Society*, vol. 106, no. 1, pp. 613–620, 2023, doi: 10.1111/jace.18769.
[43] M. Wada *et al.*, "Effect of Water Vapor on Mass Transfer in Polycrystalline $Yb_2Si_2O_7$ under Oxygen Potential Gradients at High Temperatures," *Acta Materialia*, vol. 201, pp. 373–385, Dec. 2020, doi: 10.1016/j.actamat.2020.10.002.
[44] J. Sleeper, A. Garg, V. L. Wiesner, and N. P. Bansal, "Thermochemical interactions between CMAS and $Ca_2Y_8(SiO_4)_6O_2$ apatite environmental barrier coating material," *Journal of the European Ceramic Society*, vol. 39, no. 16, pp. 5380–5390, Dec. 2019, doi: 10.1016/j.jeurceramsoc.2019.08.040.
[45] L. Barbieri, A. Corradi, and I. Lancellotti, "Thermal and chemical behaviour of different glasses containing steel fly ash and their transformation into glass-ceramics," *Journal of the European Ceramic Society*, vol. 22, no. 11, pp. 1759–1765, Oct. 2002, doi: 10.1016/S0955-2219(01)00492-7.
[46] C. Levi, J. Hutchinson, M. Vidal-Sétif, and C. Johnson, "Environmental Degradation of TBCs by Molten Deposits," *MRS Bulletin*, vol. 37, Oct. 2012, doi: 10.1557/mrs.2012.230.
[47] B. Weinzierl *et al.*, "On the visibility of airborne volcanic ash and mineral dust from the pilot's perspective in flight," *Physics and Chemistry of the Earth, Parts A/B/C*, vol. 45–46, pp. 87–102, Jan. 2012, doi: 10.1016/j.pce.2012.04.003.
[48] R. Clarkson, "Volcanic Ash Impacts on Jet Engines and Developments Since 2010, Rolls-Royce Inc. (Aero Engines)," 2019. Accessed: Jan. 07, 2021. [Online]. Available: https://www.icao.int/EURNAT/Other%20Meetings%20Seminars%20and%20Workshops/NAT%202030%20Vision%20Workshop/NAT2030%20PR10.pdf
[49] R. A. Golden, "Personal Communication," 2020.
[50] S. Krämer, J. Yang, C. G. Levi, and C. A. Johnson, "Thermochemical Interaction of Thermal Barrier Coatings with Molten CaO–MgO–Al_2O_3–SiO_2 (CMAS) Deposits," *Journal of the American Ceramic Society*, vol. 89, no. 10, pp. 3167–3175, 2006, doi: https://doi.org/10.1111/j.1551-2916.2006.01209.x.
[51] F. Wang, L. Guo, C. Wang, and F. Ye, "Calcium-magnesium-alumina-silicate (CMAS) resistance characteristics of $LnPO_4$ (Ln = Nd, Sm, Gd) thermal barrier oxides," *Journal of the European Ceramic Society*, vol. 37, no. 1, pp. 289–296, Jan. 2017, doi: 10.1016/j.jeurceramsoc.2016.08.013.
[52] L. R. Turcer, A. R. Krause, H. F. Garces, L. Zhang, and N. P. Padture, "Environmental-barrier coating ceramics for resistance against attack by molten calcia-magnesia-aluminosilicate (CMAS) glass: Part II, β-$Yb_2Si_2O_7$ and β-$Sc_2Si_2O_7$," *Journal of the European Ceramic Society*, vol. 38, no. 11, pp. 3914–3924, Sep. 2018, doi: 10.1016/j.jeurceramsoc.2018.03.010.
[53] R. I. Webster and E. J. Opila, "Mixed phase ytterbium silicate environmental-barrier coating materials for improved calcium–magnesium–alumino-silicate resistance," *Journal of Materials Research*, vol. 35, no. 17, pp. 2358–2372, 2020, doi: 10.1557/jmr.2020.151.
[54] M. Ridley, B. McFarland, C. Miller, and E. Opila, "YbPO4: A novel environmental barrier coating candidate with superior thermochemical stability," *Materialia*, vol. 21, p. 101289, 2022.

[55] A. Nieto, R. Agrawal, L. Bravo, C. Hofmeister-Mock, M. Pepi, and A. Ghoshal, “Calcia–magnesia–alumina–silicate (CMAS) attack mechanisms and roadmap towards Sandphobic thermal and environmental barrier coatings,” *International Materials Reviews*, vol. 0, no. 0, pp. 1–42, Oct. 2020, doi: 10.1080/09506608.2020.1824414.
[56] X. Hu, F. Xu, K. Li, Y. Zhang, Y. Xu, and X. Zhao, “Thermal properties and Calcium-Magnesium-Alumina-Silicate (CMAS) resistance of $LuPO_4$ as environmental barrier coatings,” *Journal of the European Ceramic Society*, vol. 40, no. 4, pp. 1471–1477, Apr. 2020, doi: 10.1016/j.jeurceramsoc.2019.11.018.
[57] L. R. Turcer and N. P. Padture, “Rare-earth pyrosilicate solid-solution environmental-barrier coating ceramics for resistance against attack by molten calcia–magnesia–aluminosilicate (CMAS) glass,” *J. Mater. Res.*, vol. 35, no. 17, pp. 2373–2384, Sep. 2020, doi: 10.1557/jmr.2020.132.
[58] J. L. Stokes, B. J. Harder, V. L. Wiesner, and D. E. Wolfe, “High-Temperature thermochemical interactions of molten silicates with $Yb_2Si_2O_7$ and $Y_2Si_2O_7$ environmental barrier coating materials,” *Journal of the European Ceramic Society*, vol. 39, no. 15, pp. 5059–5067, Dec. 2019, doi: 10.1016/j.jeurceramsoc.2019.06.051.
[59] R. Webster, “Mitigation Strategies for Calcium-Magnesium-Aluminosilicate (CMAS) Attack on Environmental Barrier Coatings,” University of Virginia, 2019. doi: 10.18130/V3-6BER-M122.
[60] Z. Yan, X. Lv, J. Zhang, Y. Qin, and C. Bai, “Influence of MgO, Al_2O_3 and CaO/SiO_2 on the viscosity of blast furnace type slag with high Al_2O_3 and 5 wt-% TiO_2,” *Canadian Metallurgical Quarterly*, vol. 55, no. 2, pp. 186–194, Apr. 2016, doi: 10.1080/00084433.2015.1126903.
[61] G. Urbain, Y. Bottinga, and P. Richet, “Viscosity of liquid silica, silicates and alumino-silicates,” *Geochimica et Cosmochimica Acta*, vol. 46, no. 6, pp. 1061–1072, Jun. 1982, doi: 10.1016/0016-7037(82)90059-X.
[62] R. W. Olesinski and G. J. Abbaschian, “The C−Si (Carbon-Silicon) System,” *Bulletin of Alloy Phase Diagrams*, no. 5, pp. 486–489, 1984.
[63] R. Hull, *Properties of crystalline silicon*. IET, 1999.
[64] W. Y. Lee, E. Lara-Curzio, and K. L. More, “Multilayered Oxide Interphase Concept for Ceramic-Matrix Composites,” *Journal of the American Ceramic Society*, vol. 81, no. 3, pp. 717–720, 1998, doi: https://doi.org/10.1111/j.1151-2916.1998.tb02396.x.
[65] M. R. Begley and J. W. Hutchinson, *The Mechanics and Reliability of Films, Multilayers and Coatings*. Cambridge University Press, 2017.
[66] A. J. Fernández-Carrión, M. Allix, and A. I. Becerro, “Thermal Expansion of Rare-Earth Pyrosilicates,” *Journal of the American Ceramic Society*, vol. 96, no. 7, pp. 2298–2305, 2013, doi: 10.1111/jace.12388.
[67] M. J. Ridley, J. Gaskins, P. Hopkins, and E. J. Opila, “Tailoring Thermal Properties of Multi-component Rare Earth Monosilicates,” *Acta Materialia*, vol. 195, pp. 698–707, Aug. 2020, doi: 10.1016/j.actamat.2020.06.012.
[68] B. T. Richards, S. Sehr, F. de Franqueville, M. R. Begley, and H. N. G. Wadley, “Fracture mechanisms of ytterbium monosilicate environmental barrier coatings during cyclic thermal exposure,” *Acta Materialia*, vol. 103, pp. 448–460, Jan. 2016, doi: 10.1016/j.actamat.2015.10.019.
[69] Y. Wang *et al.*, “Water vapor corrosion behaviors of plasma sprayed RE2SiO5 (RE = Gd, Y, Er) coatings,” *Corrosion Science*, vol. 167, p. 108529, May 2020, doi: 10.1016/j.corsci.2020.108529.
[70] M. J. Presby and B. J. Harder, “Solid particle erosion of a plasma spray – physical vapor deposition environmental barrier coating in a combustion environment,” *Ceramics International*, vol. 47, no. 17, pp. 24403–24411, Sep. 2021, doi: 10.1016/j.ceramint.2021.05.154.
[71] S. Singh, D. Singh, J. P. Singh, R. N. Singh, and J. L. Routbort, “Solid-Particle Erosion of Thin Films Deposited on Ceramics,” in *Advances in Ceramic Coatings and Ceramic-Metal Systems: Ceramic*

Engineering and Science Proceedings, John Wiley & Sons, Ltd, 2005, pp. 190–198. doi: 10.1002/9780470291238.ch23.
[72] Y. Okita, Y. Mizokami, and J. Hasegawa, "Experimental and Numerical Investigation of Environmental Barrier Coated Ceramic Matrix Composite Turbine Airfoil Erosion," *Journal of Engineering for Gas Turbines and Power*, vol. 141, no. 031013, Oct. 2018, doi: 10.1115/1.4041385.
[73] N. Kedir *et al.*, "In situ characterization of foreign object damage (FOD) in environmental-barrier-coated silicon carbide (SiC) ceramic," *Journal of the American Ceramic Society*, vol. 103, no. 8, pp. 4586–4601, 2020, doi: https://doi.org/10.1111/jace.17165.
[74] S. R. Choi, "Foreign Object Damage Phenomenon by Steel Ball Projectiles in a SiC/SiC Ceramic Matrix Composite at Ambient and Elevated Temperatures," *Journal of the American Ceramic Society*, vol. 91, no. 9, pp. 2963–2968, 2008, doi: 10.1111/j.1551-2916.2008.02498.x.
[75] K. Ogi, T. Okabe, M. Takahashi, S. Yashiro, A. Yoshimura, and T. Ogasawara, "Experimental characterization of high-speed impact damage behavior in a three-dimensionally woven SiC/SiC composite," *Composites Part A: Applied Science and Manufacturing*, vol. 41, no. 4, pp. 489–498, Apr. 2010, doi: 10.1016/j.compositesa.2009.12.005.
[76] N. Kedir *et al.*, "In situ characterization of foreign object damage (FOD) in environmental-barrier-coated silicon carbide (SiC) ceramic," *Journal of the American Ceramic Society*, vol. 103, no. 8, pp. 4586–4601, 2020, doi: 10.1111/jace.17165.
[77] N. Kedir *et al.*, "Impact damage of narrow silicon carbide (SiC) ceramics with and without environmental barrier coatings (EBCs) by various foreign object debris (FOD) simulants," *Surface and Coatings Technology*, vol. 407, p. 126779, Feb. 2021, doi: 10.1016/j.surfcoat.2020.126779.
[78] R. T. Bhatt, S. R. Choi, L. M. Cosgriff, D. S. Fox, and K. N. Lee, "Impact resistance of environmental barrier coated SiC/SiC composites," *Materials Science and Engineering: A*, vol. 476, no. 1, pp. 8–19, Mar. 2008, doi: 10.1016/j.msea.2007.04.067.
[79] L. C. Hoffman, M. J. Presby, J. L. Stokes, B. J. Harder, and J. A. Salem, "The Effect of Oxidation in Environmental Barrier Coatings Subject to Foreign Object Damage," presented at the ASME 2023 Aerospace Structures, Structural Dynamics, and Materials Conference, American Society of Mechanical Engineers Digital Collection, Oct. 2023. doi: 10.1115/SSDM2023-107437.
[80] R. B. Sosman, "System Si-SiO_2, at low p," *Trans. Br. Ceram. Soc.*, vol. 54, no. 11, pp. 655–670, 1955.
[81] N. A. Toropov and I. A. Bondar, "High-Temperature Solid Solutions of Silicates of the Rare Earth Elements," *Trans. Int. Ceram. Congr., 8th*, pp. 85–103, 1961.
[82] I. G. Talmy, D. A. Haught, and J. A. Zaykoski, "Synthesis and Properties of $BaO{\cdot}Al_2O_3{\cdot}2SiO_2$ - $SrO{\cdot}Al_2O_3{\cdot}2SiO_2$ (BAS-SAS) Ceramics," *The American Ceramic Society*, vol. 52, Art. no. CONF-940416-, Aug. 1995, Accessed: Dec. 17, 2020. [Online]. Available: https://www.osti.gov/biblio/86594
[83] D. Shin, R. Arróyave, and Z.-K. Liu, "Thermodynamic modeling of the Hf–Si–O system," *Calphad*, vol. 30, no. 4, pp. 375–386, Dec. 2006, doi: 10.1016/j.calphad.2006.08.006.
[84] Y. Hikichi and T. Nomura, "Melting Temperatures of Monazite and Xenotime," *J American Ceramic Society*, vol. 70, no. 10, p. C-252-C–253, Oct. 1987, doi: 10.1111/j.1151-2916.1987.tb04890.x.
[85] K. N. Lee *et al.*, "Upper Temperature Limit of Environmental Barrier Coatings Based on Mullite and BSAS," *Journal of the American Ceramic Society*, vol. 86, no. 8, pp. 1299–1306, 2003, doi: 10.1111/j.1151-2916.2003.tb03466.x.
[86] W. Szuszkiewicz and T. Znamierowska, "Y_2O_3-P_2O_5 Phase Diagram," *Pol. J. Chem*, vol. 63, no. 4–12, pp. 381–391, 1989.
[87] M. J. Ridley and E. J. Opila, "High-temperature water-vapor reaction mechanism of barium strontium aluminosilicate (BSAS)," *Journal of the European Ceramic Society*, vol. 42, no. 7, pp. 3305–3312, Jul. 2022, doi: 10.1016/j.jeurceramsoc.2022.02.004.
[88] E. J. Opila, "Stability of Complex Silicate Environmental Barrier Coating Candidate Materials in High-Temperature Water Vapor," Portland, OR, 2019.

[89] C. Miller and R. Webster, “Unpublished work,” University of Virginia, 2018.
[90] R. Webster and Commonwealth Center for Additive Manufacturing, “Unpublished Work,” University of Virginia, 2019.
[91] K. M. Grant, S. Krämer, J. P. A. Löfvander, and C. G. Levi, “CMAS degradation of environmental barrier coatings,” *Surface and Coatings Technology*, vol. 202, no. 4, pp. 653–657, Dec. 2007, doi: 10.1016/j.surfcoat.2007.06.045.
[92] C. B. Iyi, “CMAS reactivity with candidate ceramic oxides applicable in thermal barrier coatings,” M.S., University of California, Irvine, United States -- California, 2012. Accessed: Dec. 19, 2020. [Online]. Available: https://search.proquest.com/docview/1099071937/abstract/406DC334F1824B6FPQ/1
[93] M. A. Lamkin, “Oxygen Mobility in Silicon Dioxide and Silicate Glasses: a Review”, doi: 10.1016/0955-2219(92)90010-B.
[94] K. Ando, Y. Oishi, H. Hase, and K. Kitazawa, “Oxygen Self-Diffusion in Single-Crystal Y2O3,” *Journal of the American Ceramic Society*, vol. 66, no. 12, p. C-222-C–223, 1983, doi: https://doi.org/10.1111/j.1151-2916.1983.tb11012.x.
[95] E. B. Watson and D. J. Cherniak, “Oxygen diffusion in zircon,” *Earth and Planetary Science Letters*, vol. 148, no. 3, pp. 527–544, May 1997, doi: 10.1016/S0012-821X(97)00057-5.
[96] S. Stecura and W. J. Campbell, “Thermal Expansion and Phase Inversion of Rare-Earth Oxides,” BM-RI-5847, 4840970, Oct. 1960. doi: 10.2172/4840970.
[97] C. G. Parker, “Unpublished work, Argonne National Laboratories Advanced Photon Source, University of Virginia.” 2018.
[98] N. P. Bansal, “Solid State Synthesis and Properties of Monoclinic Celsian,” NASA Technical Memorandum 107355. Accessed: Jan. 10, 2018. [Online]. Available: https://ntrs.nasa.gov/archive/nasa/casi.ntrs.nasa.gov/19970010347.pdf
[99] Z. Ding *et al.*, “The thermal and mechanical properties of hafnium orthosilicate: Experiments and first-principles calculations,” *Materialia*, vol. 12, 2020, doi: https://doi.org/10.1016/j.mtla.2020.100793.
[100] M. Kerstan, M. Muller, and C. Russel, “High temperature thermal expansion of $BaAl_2Si_2O_8$, $CaAl_2Si_2O_8$, and $Ca_2Al_2SiO_7$ studied by high-temperature X-ray diffraction (HT-XRD),” *Solid State Sciences*, vol. 38, pp. 119–123, 2014, doi: https://doi.org/10.1016/j.solidstatesciences.2014.10.010.
[101] J. A. Deijkers, “Thermal and Environmental Barrier Coating Concepts for Silicon-based Ceramic Matrix Composites.” 2020.
[102] X. Zhong *et al.*, “Thermal shock resistance of tri-layer Yb_2SiO_5/$Yb_2Si_2O_7$/Si coating for SiC and SiC-matrix composites,” *Journal of the American Ceramic Society*, vol. 101, no. 10, pp. 4743–4752, 2018, doi: https://doi.org/10.1111/jace.15713.
[103] G. Costa, B. J. Harder, N. P. Bansal, B. A. Kowalski, and J. L. Stokes, “Thermochemistry of calcium rare-earth silicate oxyapatites,” *J Am Ceram Soc*, vol. 103, no. 2, pp. 1446–1453, Feb. 2020, doi: 10.1111/jace.16816.
[104] S. Curtarolo, G. L. W. Hart, M. B. Nardelli, N. Mingo, S. Sanvito, and O. Levy, “The high-throughput highway to computational materials design,” *Nature Mater*, vol. 12, no. 3, Art. no. 3, Mar. 2013, doi: 10.1038/nmat3568.
[105] M. V. Ayyasamy, J. A. Deijkers, H. N. G. Wadley, and P. V. Balachandran, “Density functional theory and machine learning guided search for RE2Si2O7 with targeted coefficient of thermal expansion,” *Journal of the American Ceramic Society*, vol. 103, no. 8, pp. 4489–4497, 2020, doi: 10.1111/jace.17121.

[106] Y. Liu, K. Chen, A. Kumar, and P. Patnaik, “Principles of Machine Learning and Its Application to Thermal Barrier Coatings,” *Coatings*, vol. 13, no. 7, Art. no. 7, Jul. 2023, doi: 10.3390/coatings13071140.
[107] C. J. Bodenschatz, W. A. Saidi, J. L. Stokes, R. I. Webster, and G. Costa, “Theoretical Prediction of Thermal Expansion Anisotropy for Y2Si2O7 Environmental Barrier Coatings Using a Deep Neural Network Potential and Comparison to Experiment,” *Materials*, vol. 17, no. 2, Art. no. 2, Jan. 2024, doi: 10.3390/ma17020286.
[108] K. N. Lee, “Yb2Si2O7 Environmental barrier coatings with reduced bond coat oxidation rates via chemical modifications for long life,” *Journal of the American Ceramic Society*, vol. 102, no. 3, pp. 1507–1521, 2019, doi: 10.1111/jace.15978.
[109] L. Sun *et al.*, “High temperature corrosion of (Er0.25Tm0.25Yb0.25Lu0.25)2Si2O7 environmental barrier coating material subjected to water vapor and molten calcium–magnesium–aluminosilicate (CMAS),” *Corrosion Science*, vol. 175, p. 108881, Oct. 2020, doi: 10.1016/j.corsci.2020.108881.
[110] L. R. Turcer, A. Sengupta, and N. P. Padture, “Low thermal conductivity in high-entropy rare-earth pyrosilicate solid-solutions for thermal environmental barrier coatings,” *Scripta Materialia*, vol. 191, pp. 40–45, Jan. 2021, doi: 10.1016/j.scriptamat.2020.09.008.
[111] M. J. Ridley *et al.*, “Tailoring thermal and chemical properties of a multi-component environmental barrier coating candidate (Sc0.2Nd0.2Er0.2Yb0.2Lu0.2)2Si2O7,” *Materialia*, vol. 26, p. 101557, Dec. 2022, doi: 10.1016/j.mtla.2022.101557.
[112] Y. Dong, K. Ren, Q. Wang, G. Shao, and Y. Wang, “Interaction of multicomponent disilicate (Yb0.2Y0.2Lu0.2Sc0.2Gd0.2)2Si2O7 with molten calcia-magnesia-aluminosilicate,” *J Adv Ceram*, vol. 11, no. 1, pp. 66–74, Jan. 2022, doi: 10.1007/s40145-021-0517-7.
[113] P. Zhang *et al.*, “Xenotime-type high-entropy ($Dy_{1/7}Ho_{1/7}Er_{1/7}Tm_{1/7}Yb_{1/7}Lu_{1/7}Y_{1/7}$)$PO_4$: A promising thermal/environmental barrier coating material for SiC_f/SiC ceramic matrix composites,” *Journal of Advanced Ceramics*, vol. 12, no. 5, May 2023, doi: 10.26599/JAC.2023.9220736.
[114] X. Liu *et al.*, “Effect of lattice distortion in high-entropy RE2Si2O7 and RE2SiO5 (RE=Ho, Er, Y, Yb, and Sc) on their thermal conductivity: Experimental and molecular dynamic simulation study,” *Journal of the European Ceramic Society*, vol. 43, no. 14, pp. 6407–6415, Nov. 2023, doi: 10.1016/j.jeurceramsoc.2023.06.052.